Interface characterization of Co_2MnGe/Rh_2CuSn Heusler multilayers

Ronny Knut,[1] Peter Svedlindh,[2] Oleg Mryasov,[3] Klas Gunnarsson,[2] Peter Warnicke,[4] D. A. Arena,[4] Matts Björck,[1] Andrew J. C. Dennison,[1,5] Anindita Sahoo,[6,7] Sumanta Mukherjee,[7] D. D. Sarma,[1,7] Sari Granroth,[8] Mihaela Gorgoi,[9] and Olof Karis[1]

[1]*Department of Physics and Astronomy, Uppsala University, Box 516, 75120 Uppsala, Sweden*
[2]*Solid State Physics, Department of Engineering Sciences, Uppsala University, Box 534, 751 21 Uppsala, Sweden*
[3]*Department of Physics and Astronomy and MINT Center, University of Alabama, Tuscaloosa, Tuscaloosa, Alabama 35487, USA*
[4]*National Synchrotron Light Source, Brookhaven National Laboratory, Upton, New York 11973, USA*
[5]*Institut Laue-Langevin, Grenoble 38042, France*
[6]*Department of Physics, Indian Institute of Science, Bangalore-560 012, India*
[7]*Solid State and Structural Chemistry Unit, Indian Institute of Science, Bangalore-560 012, India*
[8]*Department of Physics, University of Turku, Turku, Finland*
[9]*Helmholtz Zentrum Berlin für Materialien und Energie GmbH, BESSY II, Berlin, Germany*

(Received 30 January 2013; revised manuscript received 23 September 2013; published 10 October 2013)

To address the amount of disorder and interface diffusion induced by annealing, all-Heusler multilayer structures, consisting of ferromagnetic Co_2MnGe and nonmagnetic Rh_2CuSn layers of varying thicknesses, have been investigated by means of hard x-ray photoelectron spectroscopy and x-ray magnetic circular dichroism. We find evidence for a 4 Å thick magnetically dead layer that, together with the identified interlayer diffusion, are likely reasons for the unexpectedly small magnetoresistance found for current-perpendicular-to-plane giant magnetoresistance devices based on this all-Heusler system. We find that diffusion begins already at comparably low temperatures between 200 and 250 °C, where Mn appears to be most prone to diffusion.

DOI: 10.1103/PhysRevB.88.134407 PACS number(s): 73.20.−r, 75.20.En, 75.25.−j, 75.47.De

I. INTRODUCTION

Magnetic read head technology has experienced several large paradigm changes during the past 15 years. Anisotropic magnetoresistance read heads were surpassed by read heads based on giant magnetoresistance (GMR) in 1996, enabled by the Nobel-awarded findings of Grünberg and Fert.[1,2] Very soon after the discovery of tunnel magnetoresistance (TMR), record values of magnetoresistance (MR) were reported for sensors based on this effect. Today, TMR structures require a very thin MgO tunneling barrier (typically ∼1 nm) to achieve a sufficiently low resistance of the device and a further significant decrease of the barrier thickness appears unrealistic. It has been suggested that current-perpendicular-to-plane (CPP) GMR structures, as opposed to current in-plane structures used in first generation GMR devices, are candidates to become the next generation of MR sensors as they do not suffer resistance issues due to the all-metallic design.[3]

Heusler alloys are ternary alloys with the composition X_2YZ, where X and Y in general are two different transition metal atoms and Z is a group 3 or 4, nonmetallic element. A half-metallic character, i.e., that the density of states of the majority band is metallic while the minority band exhibits a gap at the Fermi level, was theoretically predicted for the ferromagnetic (FM) half-Heusler alloy NiMnSb,[4] followed by an extensive investigation of properties originating from this remarkable feature of the electronic structure.[5] This Heusler alloy was investigated as a candidate material for a novel CPP-GMR structure with Cu as the spacer layer.[6] Recently, Co based full-Heusler alloys renewed interest for this topic. Experimental results for two types of nonmagnetic (NM) spacers have been reported fairly recently: (i) elemental metal spacers[7,8] with a (001) texture and (ii) nonmagnetic Heusler alloy spacers[9–11] with a (110) texture. Combinations of the (001) textured FM Heusler alloys Co_2MnSi and $Co_2Fe(Si_{0.5}Al_{0.5})$ with Ag yielded MR values in excess of 28% and a change in the resistance-area product (ΔRA) of 8.8 mΩ μm^2.[7,8] More recently, enhancement of CPP-GMR up to 70% MR and a ΔRA of 16.8 mΩ μm^2 have been measured for $Co_2(Fe_{0.4}Mn_{0.6})Si$ electrodes with (001) Ag as the spacer.[12]

The half-metallic character has been theoretically predicted for ideal $L2_1$ crystals. For actual samples a certain amount of disorder is expected, which will have a negative impact on the value of the spin polarization.[13–17] The CPP-GMR in all-Heusler structures can be affected by different types of disorder, including bulk FM, bulk NM disorder, and disorder specific to FM/NM interfaces. Ambrose and Mryasov[9,10] proposed a combination of FM and NM Heusler alloys to maximize the spin asymmetry at the FM/NM interface. They argue that a structure with the appropriate combination of FM and NM Heusler alloys could provide a large, spin dependent, interface contribution to the magnetoresistance,[9,10] which, due to the non-Stoner-like spin splitting in the FM Heusler, will be less sensitive to disorder.[4,11]

For device fabrication, due to compatibility with existing processes, it would be advantageous to use the (110) textured combination of Co_2MnGe (CMG) and the nonmagnetic Heusler alloy Rh_2CuSn (RCS).[9,10] A prototype hard disk drive reader with a MR of about 7% and a ΔRA of about 4.0 mΩ μm^2 has been constructed by Nikolaev *et al.*[11] using such considerations. However, it is still much lower than for TMR structures and too low for being a viable alternative in sensor technology where MR ratios in the range of 50% at ΔRA products in the order of 0.1 Ω μm^2 are considered to be required in the roadmap for magnetic media beyond 2 TBit/in.^{2}.[3]

In this paper, we have studied the FM/NM interfaces in all-Heusler multilayer structures, with the aim to understand the

effects of postgrowth annealing on interface quality and how these depend on the individual layer thicknesses. The paper focuses on changes induced by postgrowth low temperature annealing, and it is shown that diffusion of atomic species is initiated already in the temperature range between 200 and 250 °C.

II. EXPERIMENT

We have studied multilayer samples comprising the full-Heusler compound CMG as the magnetic layer between nonmagnetic layers of the full-Heusler RCS. The samples were grown using a commercial magnetron sputtering system (Canon Anelva C7100),[11] with the following geometry: Ta(12 Å)/Ru(20 Å)/$Co_{70}Fe_{30}$(10 Å)/(CMG/RCS)$_Z$/Ru(30 Å). Here Z is the number of repetitions of the CMG/RCS bilayer. In Table I, we list the samples used in this study, differing in the combinations of CMG and RCS layer thicknesses. Three of the samples are given descriptive names since these are the most extensively studied, while the other samples will be explicitly denoted when discussed. The magnetic properties and in particular the quality of the interfaces are studied using x-ray magnetic circular dichroism (XMCD),[18,19] polarized neutron reflectivity, and superconducting quantum interference device (SQUID) magnetometry. The modifications of the interfaces were characterized by means of hard x-ray photoelectron spectroscopy (HAXPES or HX-PES, also commonly referred to as HIKE for high kinetic energy photoelectron spectroscopy).[20–22] The XMCD experiments were performed at beamlines I1011 and D1011 at the synchrotron facility MAX-lab in Lund, Sweden, with 90% and 75% circularly polarized light, respectively. All data were obtained using total electron yield. The samples were magnetized in plane after which they were measured in remanence at room temperature. All samples showed a remanent magnetization very close to the saturation magnetization. The HAXPES measurements were conducted using the HIKE station[22] at the KMC-1 beamline of the BESSY II synchrotron facility at Helmholtz Zentrum, Berlin, Germany. The samples were heated to different temperatures in the range 200–500 °C at a constant rate of 10 °C/min and kept at constant temperature for 10 min, after which the samples were cooled down to room temperature (RT) before a measurement.

Polarized neutron reflectivity was conducted up to the first multilayer Bragg peak at the SuperADAM instrument at the Institut Laue-Langevin.[23,24] The instrument was operated with a highly oriented pyrolytic graphite monochromator and two Bragg mirrors to polarize the incident beam, producing an incident wavelength of 4.4 Å. The reflected beam was analyzed with a supermirror. After each measurement the sample was annealed at the next temperature for 1 h under vacuum and was subsequently allowed to oven cool for half a day. Note that the heating protocol used for the neutron measurements is different from the one used for the other measurements, primarily due to the available hardware at the different facilities. As diffusion is found to be present already at the lowest temperatures used (100 °C), we expect that the neutron data are representative of a further progressed diffusion process, when compared to data obtained in the other measurements for the same annealing temperature.

TABLE I. Sample annotations and thicknesses of CMG and RCS layers. The CMG/RCS bilayer is repeated Z times.

Annotation	CMG (Å)	RCS (Å)	Z
Thick nonmagnetic layer	6	18	20
Thick magnetic layer	18	6	20
Thick layers	18	18	13
	24	18	11
	18	12	16
	12	18	16

III. RESULTS

Regularly, beamlines dedicated to photoemission seldom offer photon energies above 1 keV with reasonable photon intensity and resolution, which limits the electron mean free path to about 5 Å. The KMC-1 beamline at HZB delivers 2–12 keV photons with high resolution, making it ideal for studying bulk properties.[20–22] All the photoemission results described here have been obtained using a photon energy of 4 keV, giving an estimated electron mean free path of 50 Å.

As an atom in a solid is ionized by photons, the system will adapt to the presence of the positively charged ion by screening of the same. In general this involves both interatomic screening and intra-atomic relaxation. In metallic systems, a substantial fraction of the screening is due to mobile conduction electrons. The effectiveness of the screening will influence the kinetic energy of the photoelectron and hence also the measured binding energy of that electron. The screening of the ionized atom depends on the nature of the electronic structure of the local environment and the hybridization between the ionized atom and its surrounding. This is known as the chemical shift in core level spectra.[25] Here we have used the core level shifts of specific core levels of elements in both the RCS and CMG layers to study the modification of the chemical environment upon annealing. The binding energy of these core levels will be sensitive to the local environment and hence interface and bulk atoms can be distinguished, and the effect of diffusion can be studied as a function of annealing temperature.

The sample with thick CMG and RCS layers has been studied for several annealing temperatures between 200 and 500 °C, while the thick nonmagnetic layer and thick magnetic layer samples have been measured for a few selected annealing temperatures. The Rh $3d_{5/2}$ photoemission core level is shown in Fig. 1 for the sample denoted "thick layers" (see Table I). The peak clearly moves to a higher binding energy (BE) with increasing annealing temperature. In combination with the large chemical shifts found for this Rh core level, it makes it possible to reliably fit the spectra with multiple peaks, as illustrated in Fig. 2. All line shapes are set to Doniac-Sunjic type,[26] where the asymmetry and peak broadening are kept constant for every core level and are chosen so that the experimental BE shift can be well described with as few peaks as possible. A Shirley-type background was used in the fit.[27]

Each spectrum is fitted with three main peaks: one component at 306.8 eV, one at 307 eV, and one at 307.1 eV binding energy, denoted P1, P2, and P3 respectively. A fourth peak (P4) at high BE (307.4 eV) appears to be related to the two

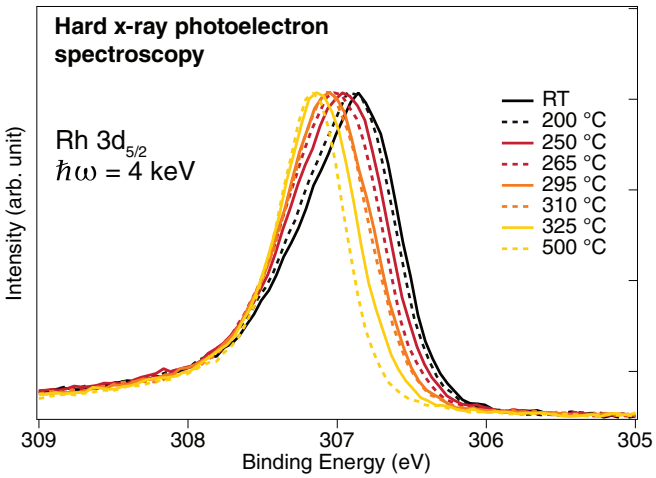

FIG. 1. (Color online) Photoemission of Rh $3d_{5/2}$ from sample CMG 18 Å/RCS 18 Å (hereafter denoted "thick layers") after different annealing temperatures. There is a peak shift to higher binding energy with increasing annealing temperature. The spectrum obtained for 265 °C (red dashed-dotted line) has been deconvoluted in Fig. 2.

main peaks at the lower BE side, since its intensity is always 14% of these peaks.

A common disorder in the full X_2YZ Heusler is X antisites in the Y atomic position. Thus, Rh antisites are a plausible explanation for this high BE peak, since it is not unlikely that 14% disorder of this type can occur.[28] As the Rh begins to migrate due to heating, the disorder is cured at the same rate.

The intensities of the three main peaks as a function of temperature, obtained by spectral deconvolution as described above, are plotted in Fig. 3. To better describe and understand the origin of these three peaks, we performed Monte Carlo simulations, where the change of the coordination number was studied when introducing random disorder as a consequence of heat treatment. A fcc lattice consisting of $26 \times 26 \times 26$ unit cells was constructed with two layers of Rh atoms, each 12 monolayers (ML) thick, representing the RCS layers.

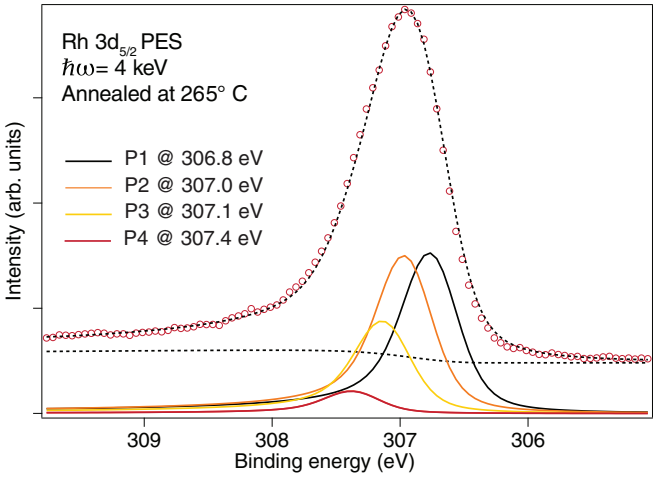

FIG. 2. (Color online) Deconvoluted spectrum of the Rh $3d_{5/2}$ core level, fitted with three main peaks and a peak at the high BE shoulder, which is always 14% of the two main peaks at the lower BE side.

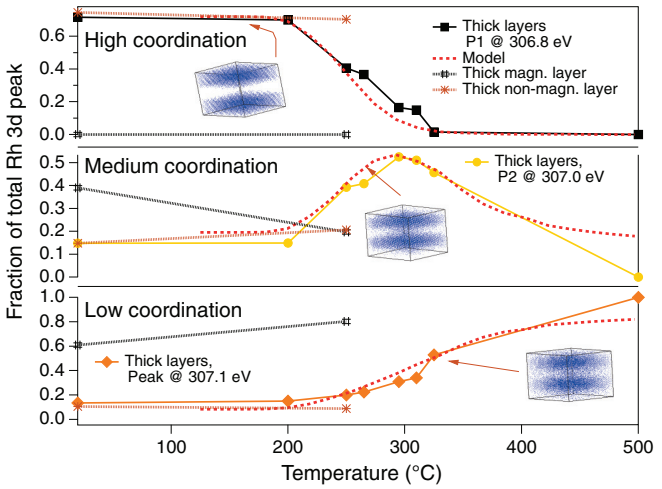

FIG. 3. (Color online) Fractions of the total peak areas of the Rh $3d_{5/2}$ core level spectrum, corresponding to the three main peaks obtained by fitting as illustrated in Fig. 2, are plotted as a function of annealing temperature. Top: High coordination component; middle: medium coordination component; bottom: low coordination component. Data for the three different samples considered are identified as indicated in the legends. The dashed lines have been obtained from Monte Carlo simulations describing the variation of the high, medium, and low coordination number cases with annealing temperature. The three lattice illustrations show the Rh distribution for different annealing temperatures.

The Rh layers are separated by 12 ML of vacant lattice positions. Both above the top Rh layer and below the bottom Rh layer there are also 8 ML of vacant lattice positions, such that the simulated diffusion will not be restricted solely to the space between the Rh layers. The diffusion of Rh atoms was simulated by generating random numbers (in the range 0–1) that should be smaller than $\exp[-\frac{E}{k_B T}]$, where E is an energy barrier, for an atom to be allowed to move. It was enough to give every atom the opportunity to move 600 times at each temperature, since the simulation results became relatively insensitive to additional moves beyond this number. The energy scale (i.e., reduced temperature) of the simulation was scaled to the experimental results.

We have only considered the Rh lattice, which in the Heusler $L2_1$ structure has a simple cubic coordination of Rh atoms. A simulation using this structure does not reproduce the experimental results accurately. A likely reason for this is the fact that the BE shift of Rh is sensitive to the Y and Z atoms in the X_2YZ Heusler structure, and a cubic lattice does not provide sufficient flexibility to encompass all the variations of nearest neighbors arising from disorder in the $L2_1$ structure. Instead we have considered a fcc structure, with 12 Rh neighbors to accommodate the variation necessary in nearest neighbor configurations to accurately model the experimental data. In a perfectly layered structure the amount of low coordinated atoms should be zero. To obtain a more realistic starting configuration, a roughness, corresponding to a displacement of randomly chosen Rh atoms at the interface, was introduced.

Illustrations of how the multilayer composition according to the simulations changes with increasing annealing temperature

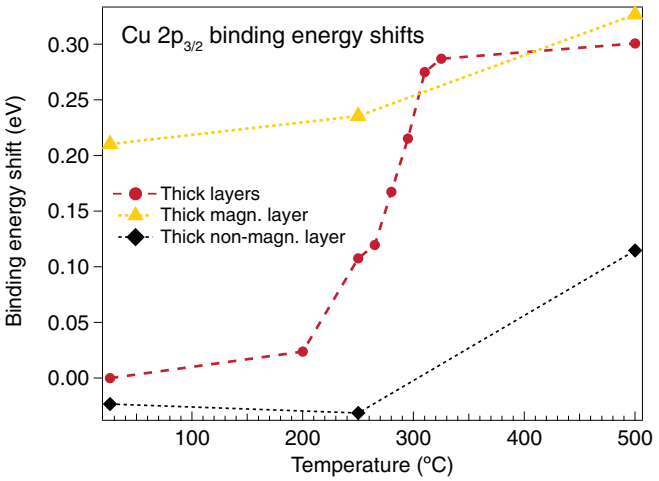

FIG. 4. (Color online) The Cu $2p_{3/2}$ core level shift as a function of annealing temperature for three samples as indicated by the legends. The BE shifts are given relative to the position of the $2p$ level for the "thick layer" sample prior to annealing. Small shifts are found for samples with thick CMG layers ("thick layers" and "thick magn. layer") already at 200 °C. We observe no chemical shift below 250 °C for the sample with the thick nonmagnetic layers, suggesting little modification below this temperature.

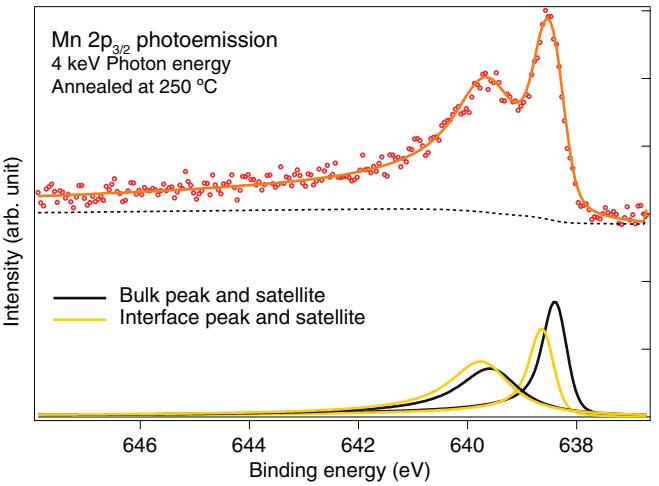

FIG. 5. (Color online) Deconvoluted Mn $2p_{3/2}$ spectrum recorded for the "thick layer" sample. The spectrum can be fitted by two components, and associated satellites, for all annealing temperatures. There is both a BE shift and a large difference in the satellite intensity between the components.

have been included as insets in Fig. 3. To obtain agreement with experiments, we found that, on average, every fourth interface Rh atom had to be moved. The fractions of atoms with 12, 8–11, and 0–7 Rh neighbors are plotted as red dashed lines in the top, middle, and bottom graphs, respectively. Using a combination of statistical methods and analysis of core level data we can thus obtain a qualitative and quantitative analysis of the distribution of Rh as a function of temperature.

The Cu $2p_{3/2}$ core level spectra, obtained for different annealing conditions, do not exhibit as large a chemical shift as the Rh $3d_{5/2}$ core level and the spectrum is always broader (not shown). These factors make it more difficult to use data for the Cu $2p$ level for quantitative analysis such as for Rh as described above. By only considering the centroid of the spectrum fitted with a single Doniac-Sunjic profile, we can, however, assign a chemical shift for each annealing temperature and sample. The result is presented in Fig. 4. The core level shift is given relative to the position of the $2p$ level for the "thick layer" sample prior to annealing, which is thus set to zero. We observe that the sample with thick magnetic CMG layers and thin RCS layers exhibits a significant shift already before annealing. We therefore conclude that data for both the Cu and Rh core levels indicate that samples with a thin RCS layer have, as expected, a low fraction of ordered bulklike RCS. In contrast, we find that the BE of the Cu $2p$ core level for the sample with the thick RCS layer is very similar to the reference level of the "thick layer" sample. The temperature dependence of the Cu $2p$ core level shift suggests that modifications occur already around 200 °C. However, we find that the core level shift of the "thick layer" sample exhibits an abrupt transition in the temperature range 200–300 °C.

The Mn $2p_{3/2}$ spectra have been fitted by two peaks that both exhibit strong satellite structures, as illustrated in Fig. 5, where the results for the "thick layer" sample annealed at 250 °C is shown. Also here, Shirley-type backgrounds were used. In the fitting procedure, the intensity of the satellite was kept constant relative to that of the main line. The main peak at ∼638.4 eV is attributed to the interior of the layer (bulk peak), while the peak at ∼638.6 eV is attributed to the interface. The fraction of each peak as a function of temperature is shown in Fig. 6. Similar to what was found above for Cu, there are also differences in the temperature dependence of the core level shift for the Mn $2p$ core level depending on the thickness of the adjacent layer. Also, as for Cu $2p$, we observe changes for the Mn $2p$ core level already for an annealing temperature of 200 °C. The bulk component is smaller for the "thick magnetic layer" sample which has a thinner RCS layer (triangles), which would suggest that the interface quality is lower for thinner RCS layers. As expected, the bulk component is also smaller

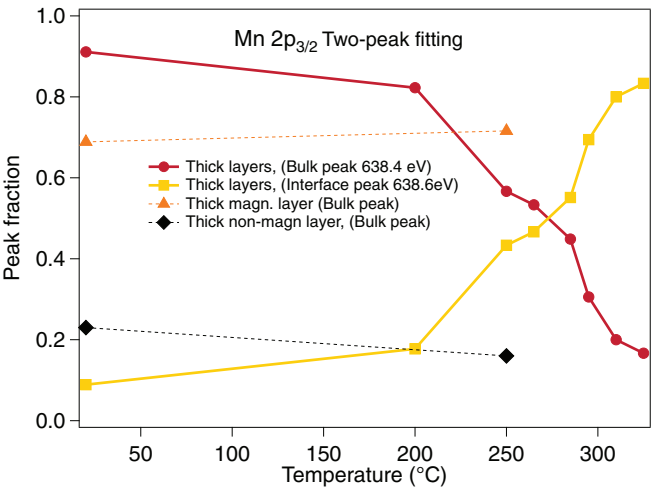

FIG. 6. (Color online) The intensity of the bulk (circles) and interface (squares) peaks, derived from fits such as those illustrated in Fig. 5, are plotted as a function of annealing temperature for the "thick layer" sample. Only the bulk component is plotted for the other samples (triangles and diamonds).

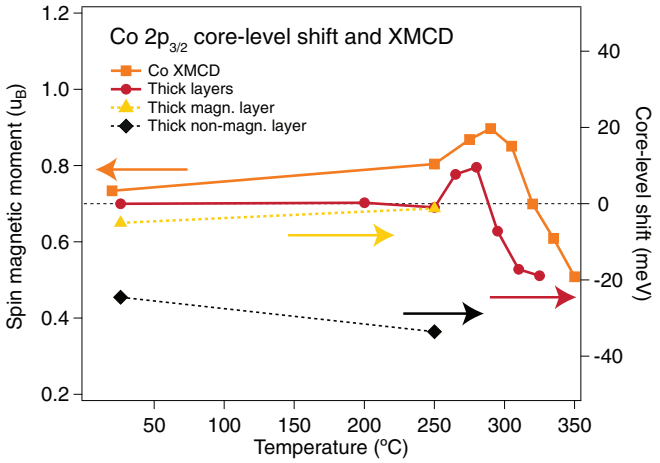

FIG. 7. (Color online) The Co XMCD spin magnetic moment is plotted on the left scale. On the right scale we have plotted the chemical shift of the Co $2p_{3/2}$ core level. The behavior of the chemical shift and magnetic moment is very similar.

for the "thick nonmagnetic layer" sample with a thinner CMG layer (diamonds).

In Fig. 7 we show the chemical shift of the Co $2p_{3/2}$ core level as a function of annealing temperature. As for Cu, the core level shift was obtained by fitting a single Doniac-Sunjic line with a Shirley background to the data at each temperature and sample. The samples with thick CMG layers, i.e., the "thick layers" and "thick magnetic layer," exhibit a negligible chemical shift of the Co $2p_{3/2}$ core level up to 250 °C, suggesting little modification at the X sites below this temperature. Between 250 and 280 °C, we find an increasing positive shift. For annealing temperatures above 280 °C, the chemical shift becomes negative and we observe an increasing negative shift in the interval 280–325 °C.

The spin magnetic moment of Co, as obtained from an XMCD,[18,19] is also shown in Fig. 7. A $3d$-hole count of 2.2 for Co and 4.2 for Mn (Refs. 29 and 30) was used for extracting the magnetic moments from the XMCD sum rules.[18,19] The qualitative behavior is very similar to the annealing temperature dependence of the core level shift, which also shows an increase in the same temperature range, followed by a decrease. The variation in both the spin magnetic moment, obtained by means of XMCD sum-rule analysis, and the chemical shift suggests that different diffusion processes occur at two different temperature ranges. In the high temperature range (above 280 °C), the BE decrease of the Co $2p$ core level can be attributed to interlayer diffusion. In the temperature range where we observe an increase of Co $2p$ BE (250–280 °C), the Co diffusion could be related to the formation of Co_{Mn} antisites, since Mn appears to be highly mobile already at these temperatures, as discussed above. According to *ab initio* calculations, antisites where Co atoms occupy Mn sites are expected to occur in CMG Heusler alloys[11,16,31] and will increase the Co spin magnetic moment by 32% but will be detrimental for the spin polarization.[16,31] We thus conclude that such antisites could explain the observed increase of the Co spin magnetic moment found by XMCD, though it cannot be excluded that the variation of the derived spin magnetic moment is, in part, an effect of changes in the number of $3d$ holes.

The sample consisting of 24 Å CMG/ 18 Å RCS was studied with neutron reflectivity to complement the spectroscopic methods. The sample was chosen due to its large layer thicknesses, which made it suitable for neutron reflectivity measurements. The data were analyzed with the GENX program[32] by co-refining all data sets up to 300 °C, keeping the same parameters for all temperatures except for the roughness of the RCS, CMG, and the capping layers. In addition, the magnetic moment for the CMG layer was allowed to vary. For the four refined data sets, up to a temperature of 250 °C, there was a total of 51 free parameters yielding a fit with a crystallographic $R1$ factor of 5.7%. Porod plots of the fits for the reflectivities of both measured neutron spin states are displayed in Fig. 8 (left). In all cases, the poor contrast between the layers for spin-up neutrons (represented by yellow/gray circles) leads to a greatly reduced Bragg peak intensity. For spin-down neutrons (red/black circles), the Bragg peak is clearly visible. The parameters of interest in this study are extracted from these fits; the roughness of the multilayer interfaces and the magnetic moment of the CMG layer can be seen in Fig. 8 (right). It should be noted that after an anneal to 300 °C the multilayer Bragg peak has disappeared completely, indicating a total intermixing of the layered structure (not shown). This temperature can consequently not be modeled by merely allowing the roughnesses to vary as there are no interfaces left, consequently, it is left out of the discussion of the reflectivity data. However, the large changes seen as the annealing temperature increases to 300 °C are in agreement with the HAXPES data that also show layer interdiffusion at these temperatures. The first rise in the roughness of the RCS on CMG interface in Fig. 8 (right) is in accordance with the weak intermixing seen for the Mn and Cu core levels. The intermixing is mostly localized to one of the interfaces in the multilayer structure, RCS on CMG, and starts already at around a temperature of 100 °C. We again note the distinction between the protocols used for heating due to differences in the hardware used. The longer annealing time used for the samples used in the neutron measurements are likely giving rise to the apparent higher degree of interdiffusion indicated by the neutron data.

The saturation magnetic moments for all samples were obtained with SQUID magnetometry. The 6 Å CMG/ 18 Å RCS sample, which shows no remanence in XMCD, was used to obtain the magnetization of the FeCo seed layer by assuming that only this layer contributes to the remanent magnetization obtained from the SQUID magnetometry. The magnetization of $Fe_{70}Co_{30}$ was found to be 1.5×10^6 A/m, which is close to the bulk value of 1.74×10^6 A/m estimated from the Slater-Pauling curve.[33] To account for the magnetization obtained by means of SQUID magnetometry, we adopt a model which includes a magnetically dead region in the CMG. If one assumes a theoretical magnetic moment of $5\mu_B$/f.u. in the CMG layer, one finds that the thickness of this magnetically dead region will have to increase from 5 to 10 Å as the CMG layer thickness increases from 12 to 24 Å. However, as illustrated in Fig. 9, if one assumes a magnetic moment of $4\mu_B$/f.u., we find that the required thickness of the dead layer is much less dependent on the CMG/RCS thickness,

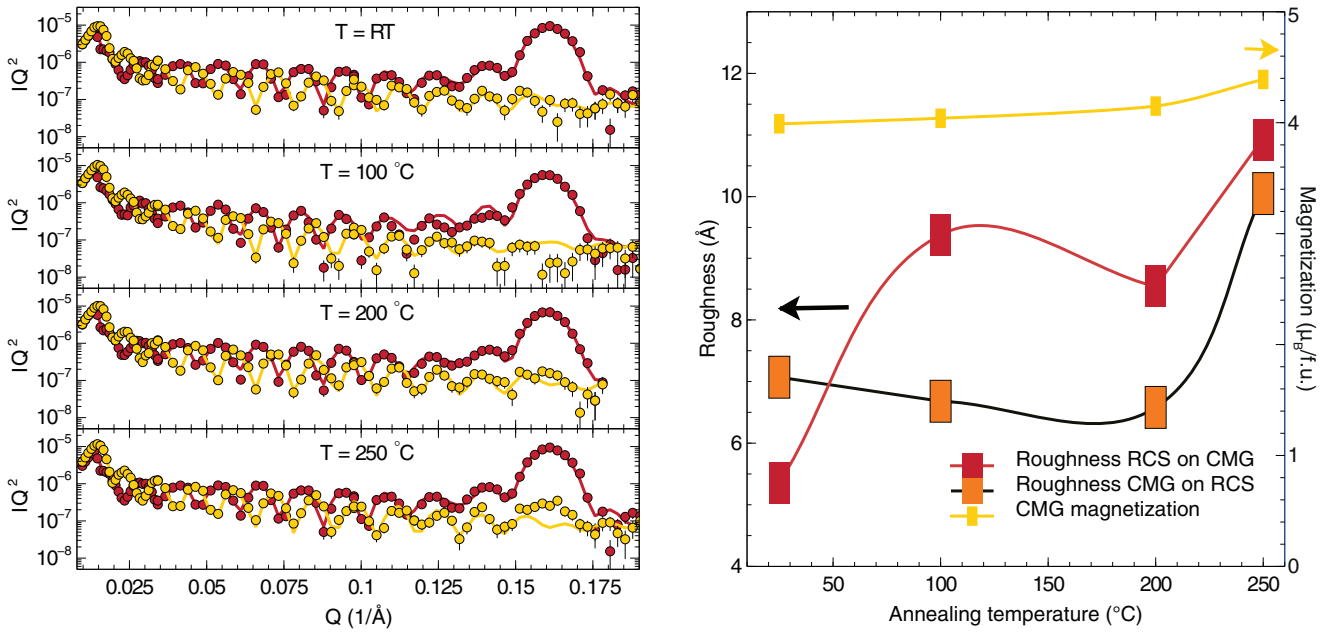

FIG. 8. (Color online) Left: Polarized neutron reflectivity data for the 24 Å CMG/ 18 Å RCS sample with data for spin-up and spin-down polarization states, and their lines of best fit using the structural/magnetic model displayed as yellow (gray) and red (black) colors, respectively. Right: The interface roughness and magnetic moment obtained from the refinement using GENX (Ref. 32). The roughness of RCS grown on CMG is very sensitive to annealing already at 100 °C.

with an approximately constant thickness of about 4 Å. This corresponds well to the magnetic moment found by neutron reflectivity.

In Fig. 9, the dead layer thickness for samples with 18 Å CMG and a varying RCS layer is plotted as circles. For samples with 18 Å RCS and a varying CMG layer, the dead layer thickness is plotted as solid diamonds. A small increase in the dead layer thickness is found for samples annealed to 250 °C (open diamonds).

The XMCD Co spin magnetic moments as functions of CMG and RCS layer thicknesses are shown in Fig. 10. In the upper graph we give the data for a constant CMG layer thickness of 18 Å varying the RCS layer thickness, while for

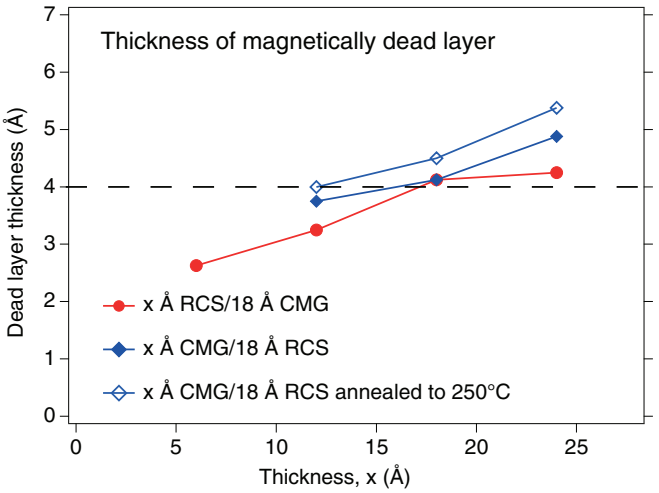

FIG. 9. (Color online) Estimated thickness of the magnetically dead layer for different layer thicknesses obtained from SQUID magnetometry. Circles: The thickness for the CMG layer has been kept constant at 18 Å, while the RCS layer thickness is varied between 6 and 24 Å. Solid diamonds: The RCS layer thickness is 18 Å, while the CMG thickness is varied between 12 and 24 Å. Open diamonds: As previous data, but the samples have been annealed at 250 °C. The dead layer thickness is relatively insensitive to the thickness of the layers.

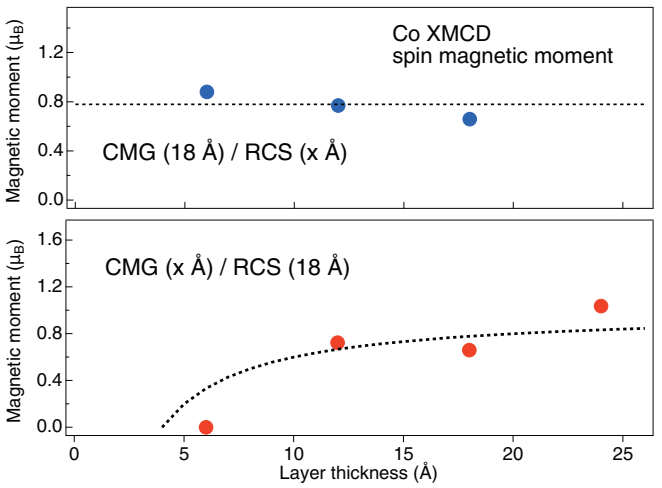

FIG. 10. (Color online) The Co spin magnetic moment for different CMG and RCS layer thicknesses before annealing. The top graph shows data for a constant CMG layer thickness of 18 Å varying the RCS layer thickness, while the lower graph shows data for a constant RCS layer thickness of 18 Å varying the CMG layer thickness. The dashed lines correspond to fits assuming a 4 Å magnetically dead layer and a Co spin magnetic moment of $1\mu_B$/Co atom for the two situations.

the lower graph we vary the CMG layer thickness, keeping the RCS layer thickness constant at 18 Å. The dashed lines correspond to the average Co moment in the CMG layer, assuming a 4 Å thick magnetically dead layer and a Co spin moment of $1\mu_B$/Co atom[34,35] in the remaining part of the CMG layer. In the top graph the fit is consistent with a constant magnetic moment since the thickness of the magnetic layer does not change. In the lower graph we observe an increase of the magnetic moment with increasing CMG thickness.

The Mn XMCD was generally hampered by large background contributions, and sufficient data quality for sum-rule analysis was only obtained for the "thick magnetic layer" sample. Taking the 4 Å magnetically dead layer into consideration, we obtain a Mn spin magnetic moment of $1.98\mu_B$. This gives a total magnetic moment of $3.93\mu_B$ in the unit cell, which is very close to the magnetic moment obtained from neutron reflectivity. However, using the sum rules for Mn is not straightforward due to mixing of the Mn L_2 and L_3 edges. A correction factor of 1.47 has been proposed,[36] but Saito *et al.*[35] found that omitting the correction factor gives a more reasonable Mn spin magnetic moment. Other studies have found that the magnetic moment of Mn is generally smaller for thin layers compared to bulk, while the Co magnetic moment increases.[34,35] This can be explained by the disorder in thin films giving an increased magnetic moment for Co_{Mn} while Mn_{Co} is antiferromagnetically coupled to its nearest neighbors and will hence lower the saturation magnetization of the film.[31]

IV. DISCUSSION AND CONCLUSIONS

The CMG and RCS Heusler alloys were chosen due to the band matching criteria, proposed theoretically, to provide a large spin asymmetry. This requires high quality interfaces which are robust to low temperature annealing, $\simeq$250 °C. This temperature is set by requirements in the fabrication processes of actual devices. We have studied the properties of interfaces using hard x-ray photoelectron spectroscopy, x-ray magnetic circular dichroism, and polarized neutron reflectivity for different thicknesses of both RCS and CMG layers, as deposited and after annealing to temperatures up to 500 °C. As expected, we generally find that layers as thin as 6 Å show little bulklike contributions. For as-deposited samples with thicker RCS layers, we find that Rh has about 10% of the atoms in a low coordinated state before heat treatment, which is in accordance with neutron reflectivity data suggesting a roughness of 6 Å at the interfaces. Hard x-ray photoelectron spectroscopy results further indicate small changes in the RCS and CMG layer already after annealing to 200 °C, which can in particular be observed in the data obtained for Mn and Cu core levels. The implications of these changes are likely not severe for device functionality. Polarized neutron reflectivity indicates an asymmetric behavior at the interfaces, where an increase in the interface roughness is found for the interface of RCS on CMG for an annealing temperature of 200 °C, while the CMG on RCS interface appears to be more stable. However, for annealing temperatures above 200 °C, a strong intermixing is found for Rh, Cu, and Mn, and a large increase of interface roughness is observed in the neutron data. The Co appears relatively stable at temperatures up to 250 °C. However, we find indications of Co_{Mn} antisite formation between 250 and 300 °C. These antisites have a negative impact on the spin polarization of the material. Antisite defects are well known to exist in Heusler alloys and are considered to be cured by high temperature annealing ($\sim$500 °C for bulk materials). For the layered structures investigated here, the Mn diffusion observed above 200 °C is a likely explanation as to why Co_{Mn} antisites are created rather than cured around 280 °C. We should point out that Varaprasad *et al.*[28] showed that the amount of Co_{Mn} antisites can be reduced by exchanging 25% of the Ge with Ga. The thickness dependence of the net magnetization and the atomic magnetic moments can be explained reasonably well by assuming a 4 Å magnetically dead layer in CMG. The total magnetization of CMG is about $4\mu_B$/f.u., which is lower than the bulk value of $5\mu_B$/f.u. This is probably due to Mn_{Co} antisites which couple antiferromagnetically to their nearest neighbors, while Co_{Mn} antisites give an increase in magnetic moment.

In conclusion, we have shown how characterization of the electronic structure, in combination with magnetometry and spin polarized neutron reflectivity, can address modifications in all-Heulser multilayers structures, specifically designed to model interfaces in actual current-perpendicular-to-plane giant magnetoresistance devices. The existence of Co_{Mn} antisites, which have a negative impact on the spin polarization, are found. Annealing appears rather to promote the creation of such antisites. Additionally, our study shows that the stability of the interfaces at temperatures between 200 and 300 °C, as well as the existence of a 4 Å magnetically dead layer, will be a major issue for device fabrication using this all-Heusler combination.

ACKNOWLEDGMENTS

This work was supported by the Swedish Research Council (VR) and the Swedish Foundation for International Cooperation in Research and Higher Education (STINT). VR is also acknowledged for their financial support of SuperAdam. We acknowledge the Helmholtz-Zentrum Berlin–Electron storage ring BESSY II for provision of synchrotron radiation at beamline KMC-1. We also would like to thank M. Mertin for assistance. The research leading to these results has received funding from the European Community's Seventh Framework Programme (FP7/2007-2013) under Grant Agreement No. 226716. O.K. gratefully acknowledges the support of the Göran Gustavsson Foundation.

[1] M. N. Baibich, J. M. Broto, A. Fert, F. Nguyen Van Dau, F. Petroff, P. Eitenne, G. Creuzet, A. Friederich, and J. Chazelas, Phys. Rev. Lett. **61**, 2472 (1988).

[2] G. Binasch, P. Grünberg, F. Saurenbach, and W. Zinn, Phys. Rev. B **39**, 4828 (1989).

[3] M. Takagishi, K. Yamada, H. Iwasaki, H. N. Fuke, and S. Hashimoto, IEEE Trans. Magn. **46**, 2086 (2010).

[4] R. A. de Groot, F. M. Mueller, P. G. van Engen, and K. H. J. Buschow, Phys. Rev. Lett. **50**, 2024 (1983).

[5]M. I. Katsnelson, V. Y. Irkhin, L. Chioncel, A. I. Lichtenstein, and R. A. de Groot, Rev. Mod. Phys. **80**, 315 (2008).
[6]J. Caballero, Y. Park, J. Childress, J. Bass, W. Chiang, A. Reilly, W. Pratt, and F. Petroff, J. Vac. Sci. Technol. A **16**, 1801 (1998).
[7]T. Iwase, Y. Sakuraba, S. Bosu, K. Saito, S. Mitani, and K. Takanashi, Appl. Phys. Express **2**, 063003 (2009).
[8]T. M. Nakatani, T. Furubayashi, S. Kasai, H. Sukegawa, Y. K. Takahashi, S. Mitani, and K. Hono, Appl. Phys. Lett. **96**, 212501 (2010).
[9]T. Ambrose and O. Mryasov, *Half-Metallic Alloys: Fundamentals and Applications* (Springer, Berlin, 2005).
[10]T. Ambrose and O. Mryasov, U.S. Patent No. 6,876,522 (5 April 2005).
[11]K. Nikolaev, P. Kolbo, T. Pokhil, X. Peng, Y. Chen, T. Ambrose, and O. Mryasov, Appl. Phys. Lett. **94**, 222501 (2009).
[12]J. Sato, M. Oogane, H. Naganuma, and Y. Ando, Appl. Phys. Express **4**, 113005 (2011).
[13]M. Carey *et al.*, Appl. Phys. Lett. **85**, 4442 (2004).
[14]K. Ozdogan and I. Galanakis, J. Appl. Phys. **110**, 076101 (2011).
[15]I. Galanakis, K. Özdoğan, and E. Şaşioğlu, in *Advances in Nanoscale Magnetism*, edited by B. Aktas and F. Mikailov, Springer Proceedings in Physics Vol. 122 (Springer, Berlin, 2009), p. 1.
[16]B. Ravel, J. Cross, M. Raphael, V. Harris, R. Ramesh, and V. Saraf, Appl. Phys. Lett. **81**, 2812 (2002).
[17]M. Ležaić, P. Mavropoulos, S. Blügel, and H. Ebert, Phys. Rev. B **83**, 094434 (2011).
[18]P. Carra, B. T. Thole, M. Altarelli, and X. Wang, Phys. Rev. Lett. **70**, 694 (1993).
[19]B. T. Thole, P. Carra, F. Sette, and G. van der Laan, Phys. Rev. Lett. **68**, 1943 (1992).
[20]E. Holmström, W. Olovsson, I. A. Abrikosov, A. M. N. Niklasson, B. Johansson, M. Gorgoi, O. Karis, S. Svensson, F. Schäfers, W. Braun, G. Öhrwall, G. Andersson, M. Marcellini, and W. Eberhardt, Phys. Rev. Lett. **97**, 266106 (2006).
[21]S. Granroth, R. Knut, M. Marcellini, G. Andersson, S. Svensson, O. Karis, M. Gorgoi, F. Schäfers, W. Braun, W. Eberhardt, W. Olovsson, E. Holmström, and N. Mårtensson, Phys. Rev. B **80**, 094104 (2009).
[22]M. Gorgoi, S. Svensson, F. Schäfers, G. Öhrwall, M. Mertin, P. Bressler, O. Karis, H. Siegbahn, A. Sandell, H. Rensmo, W. Doherty, C. Jung, W. Braun, and W. Eberhardt, Nucl. Instrum. Methods . Phys. Res., Sect. A **601**, 48 (2009), special issue in honor of Professor Kai Siegbahn.
[23]D. Mishra, M. J. Benitez, O. Petracic, G. A. B. Confalonieri, P. Szary, F. Brüssing, K. Theis-Bröhl, A. Devishvili, A. Vorobiev, O. Konovalov, M. Paulus, C. Sternemann, B. P. Toperverg, and H. Zabel, Nanotechnology **23**, 055707 (2012).
[24]M. Wolff, K. Zhernenkov, and H. Zabel, Thin Solid Films **515**, 5712 (2007).
[25]B. Johansson and N. Mårtensson, Phys. Rev. B **21**, 4427 (1980).
[26]S. Doniach and M. Sunjic, J. Phys. C: Solid State Phys. **3**, 285 (1970).
[27]J. Végh, J. Electron Spectrosc. Relat. Phenom. **151**, 159 (2006), and references therein.
[28]B. Varaprasad, A. Rajanikanth, Y. Takahashi, and K. Hono, Appl. Phys. Express **3**, 023002 (2010).
[29]V. N. Antonov, O. Jepsen, A. N. Yaresko, and A. P. Shpak, J. Appl. Phys. **100**, 043711 (2006).
[30]J. Grabis, A. Bergmann, A. Nefedov, K. Westerholt, and H. Zabel, Phys. Rev. B **72**, 024437 (2005).
[31]S. Picozzi, A. Continenza, and A. J. Freeman, Phys. Rev. B **69**, 094423 (2004).
[32]M. Björck and G. Andersson, J. Appl. Crystallogr. **40**, 1174 (2007).
[33]R. Bozorth, *Ferromagnetism* (Van Nostrand, New York, 1951), p. 441.
[34]D. Asakura, T. Koide, S. Yamamoto, K. Tsuchiya, T. Shioya, K. Amemiya, V. R. Singh, T. Kataoka, Y. Yamazaki, Y. Sakamoto, A. Fujimori, T. Taira, and M. Yamamoto, Phys. Rev. B **82**, 184419 (2010).
[35]T. Saito, T. Katayama, T. Ishikawa, M. Yamamoto, D. Asakura, T. Koide, Y. Miura, and M. Shirai, Phys. Rev. B **81**, 144417 (2010).
[36]Y. Teramura, A. Tanaka, and T. Jo, J. Phys. Soc. Jpn. **65**, 1053 (1996).